# Supplemental Material: Linking the dielectric Debye process in mono-alcohols to their density fluctuations.

## I. EXPERIMENTAL DETAILS

The samples were purchased from Sigma-Aldrich at purity $\geq$ 99.6 % for 2-ethyl-1-hexanol and purity $\geq$ 99 % for 4-methyl-3-heptanol (mixture of isomers). The samples were used as received.

All bulk and shear modulus measurements were carried out in the same experimental set-up, at the same temperatures (however, the shear modulus measurement included some lower temperatures than the bulk modulus measurement) and frequencies.

The set-up includes a custom-built closed-cycle cryostat able to keep the temperature stable within about 1 mK. The electronics of the set-up consist of a custom-built generator for frequencies up to 100 Hz, a HP 3458A multimeter (measuring at low frequencies) and an Agilent E4980A Precision LCR meter (measuring frequencies up to 2 MHz).

Further details of the experimental set-up is given in Refs. [S1, S2]. Details of measuring techniques in given Ref. [S3] (shear modulus technique) and Refs. [S4, S5] (bulk modulus technique).

## II. SHEAR MECHANICAL DATA

Shear modulus data for 2-ethyl-1-hexanol (2E1H) was published in Refs. S6 and S7, but rather than using the old data we decided to measure again. This was done for several reasons: 1) previous measurements were carried out at slightly different temperatures 2) measurements were performed in a different experimental set-up 3) for the data extraction procedure described in below it was a "cleaner" implementation when data points are measured at identical frequencies as in the bulk modulus measurement instead of shifting a master curve in frequency and then interpolating between frequencies to match the bulk modulus measurement.

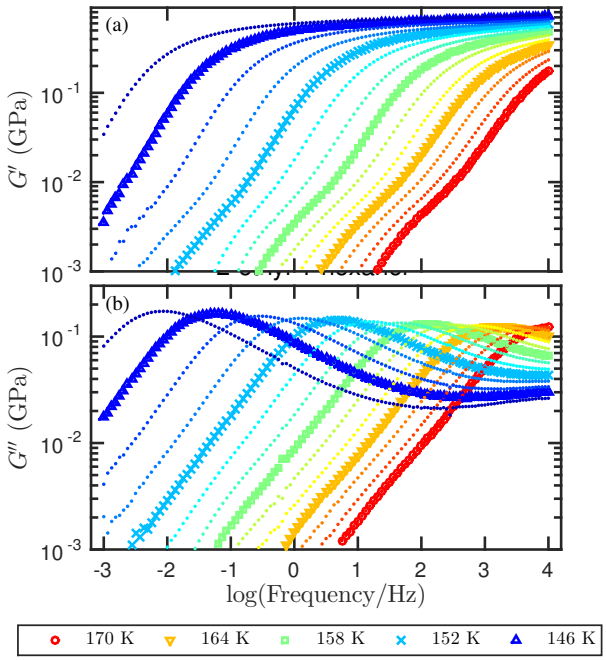


FIG. S1: Real (a) and imaginary (b) part of the shear modulus of 2E1H at temperatures from 170 K to 144 K in steps of 2 K.

Shear modulus was thus re-measured in the same experimental set-up as the bulk modulus, changing only the measuring cell while the cryostat, cryostat stick, and electronics were identical under the two measurements. Data are shown in Fig. S1. The data agree well with previously published shear modulus data [S6, S7] for 2E1H.

Previously published shear modulus data for 4-methyl-3-heptanol (4M3H) [S7] were taken in the same experimental setup as the bulk modulus data, so there was no need to re-measure the shear modulus for 4M3H.

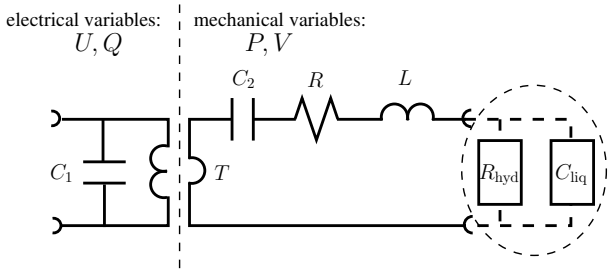


FIG. S2: Model of the PBG. The transformer (also marked by a vertical dashed line) separates the electrical and the mechanical side of the model. The encircled area shows the part that is only present when the PBG is filled. An empty transducer corresponds to the mechanical port of the model being shorted. The electrical side (left of the transformer, $T$) the capacitance $C_1$ models the electrical capacitance of the piezo-electric ceramic shell. On the mechanical side (right of the transformer) the $RCL$-circuit models the mechanical properties of the ceramics. The transformer models the piezo-electric conversion of the applied electrical field to mechanical displacement. When there is liquid in the PBG, there is an extra (complex) capacitance due to the liquid ($C_{\mathrm{liq}}$), and an extra (complex) resistor ($R_{\mathrm{hyd}}$) modeling the flow in the filling pipe.

## III. MODEL FOR THE PBG

This section gives the background for the data treatment of the bulk modulus data and is essential to the conclusions drawn.

The PBG can be modeled by an electrical diagram, where each element represents a particular property of the PBG [S5]. Such a diagram is essentially a simple way of constructing the constitutive equations of the PBG in a physically consistent manner.

Figure S2 shows the electrical diagram model of the PBG. The model has an electrical side (left) and a mechanical side (right) where the volume $V$ plays the role of electrical charge $Q$ and the pressure $P$ is the equivalent of the voltage $U$ on the electrical side. The transformer (separating the two sides of the diagram) represents the piezo-electric conversion of electrical voltage to a mechanical displacement. The capacitance on the electrical side $C_1$ models the electrical capacitance of the piezo-electric ceramic shell. On the mechanical side, the $RCL$-circuit models the mechanical properties of the ceramics. When there is liquid in the transducer, an extra (complex) capacitance due to the liquid ($C_{\mathrm{liq}}$), and an extra (complex) resistor ($R_{\mathrm{hyd}}$) modeling the flow in the filling pipe is added to the model.

Using the simple rules for adding electrical network elements (impedances added in series, admittances added in parallel), we arrive at the following expression for the measured capacitance, i.e., the response when measured at the electrical side of the model

$$C_{\mathrm{m}}(\omega) = C_1 + T^2 \frac{1}{\frac{1}{C_2} + i\omega R - \omega^2 L + \left[\frac{1}{\frac{1}{i\omega R_h} + C_{\mathrm{liq}}}\right]}\,, \tag{S1}$$

where the expression in the square brackets only is present if the PBG is filled with liquid.

Equation (S1) can be rewritten in some convenient variables: the clamped (high-frequency limit) capacitance $C_{cl} = C_1$, the free (low-frequency limit) capacitance $C_{fr} = C_1 + T^2 C_2$, the resonance frequency $\omega_0 = \sqrt{1/LC_2}$, and the quality factor $Q = 1/R\sqrt{L/C_2}$. The rewritten expression is then

$$C_{\mathrm{m}}(\omega) = C_{cl} + \frac{C_{fr} - C_{cl}}{1 + i\frac{\omega}{\omega_0}\frac{1}{Q} - \frac{\omega^2}{\omega_0^2} + \left[\frac{C_2}{\frac{1}{i\omega R_{\mathrm{hyd}}} + C_{\mathrm{liq}}}\right]}\,. \tag{S2}$$

The hydrodynamic flow resistance $R_{\mathrm{hyd}}$ is proportional to the shear viscosity, $\eta_G$. Assuming a Poiseuille flow (see Sec. IV below), the factor of proportionality is given by

$$A = \frac{8L}{\pi a^4}\,, \tag{S3}$$

where $L$ is the length of the pipe and $a$ is the radius. Inserting this and rearranging Eq. (S2) to isolate $C_{\mathrm{liq}}$ (which is

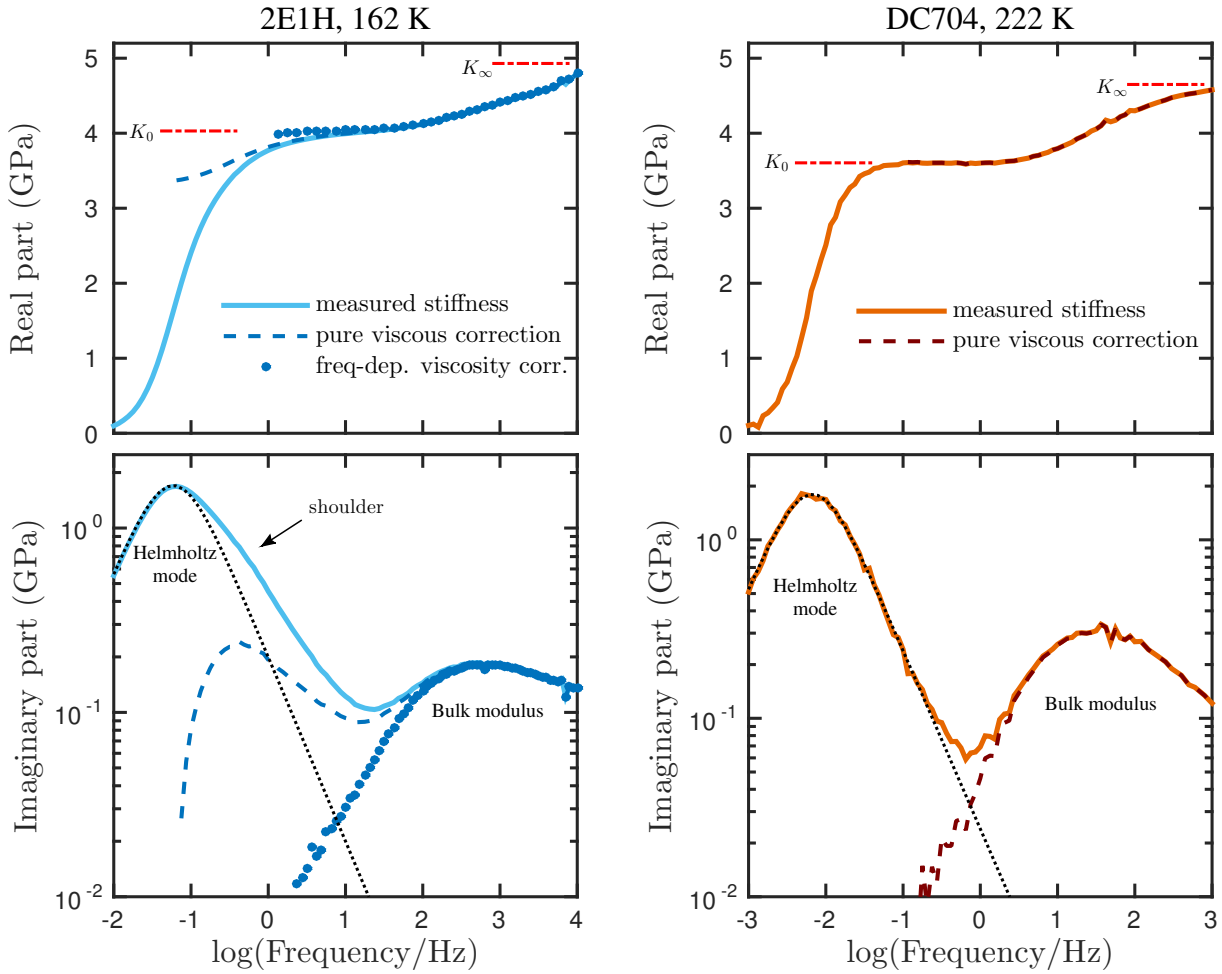


FIG. S3: Real and imaginary parts of the measured stiffness of 2-ethyl-1-hexanol (2E1H) and the silicone oil, tetraphenyl-tetramethyl-trisiloxane (DC704). At low frequencies, the real part of the measured stiffness goes to zero (solid line), because the liquid has time to flow in and out of the small filling tube and thus there is no resistance to the deformation of the piezo-ceramic shell. In the imaginary part this is seen as a peak, the Helmholtz mode. In the real part the limiting low- and high-frequency moduli, $K_0$ and $K_\infty$ are indicated by red dashed lines. The simple, purely viscous correction (see Eq. (S1)) is shown in both real and imaginary parts as the dashed line. It corresponds to the "subtraction" of the dotted black line in the imaginary part. While this procedure works perfectly in non-associated molecular liquids, extending the frequency range of the bulk modulus by approximately 1 decade (shown here for DC704), it clearly leads to an extra peak in the imaginary part and a corresponding extra step in the real part in the case of 2E1H. This apparent extra process comes from the "shoulder" indicated by an arrow in the imaginary part of the 2E1H spectrum. The shoulder is consistent with the slow polymer-like frequency dependence of the shear viscosity in 2E1H recently documented [S7] influencing the Poiseuille flow. Inserting the measured frequency-dependent shear modulus in the model (Eq. (S5)) completely removes this shoulder and reveals the true bulk modulus (blue circles).

the signal we are after), we arrive at

$$C_{\rm liq}(\omega) = C_2 \left( F^{-1} - 1 - i\frac{\omega}{\omega_0}\frac{1}{Q} + \frac{\omega^2}{\omega_0^2} \right)^{-1} - \frac{1}{i\omega A \eta_G} \tag{S4}$$

where $F = \frac{C_{\rm m}(\omega) - C_{cl}}{C_{fr} - C_{cl}}$.

For liquids that display a "simple" low-frequency behavior in the shear modulus (e.g., most non-associated molecular liquids), it is sufficient to plug in the DC viscosity in the model (corresponding to a pure resistor in the network in place of the $R_{\rm hyd}$-box in Fig. S2). A more sophisticated model takes the frequency-dependence of the viscosity into account. This could either be done by putting in a more complicated model for $R_{\rm hyd}$, but one could also plug in the

actual measured shear viscosity. Since $\eta_G = \frac{G}{i\omega}$, where $G$ is the complex shear modulus we finally arrive at

$$C_{\rm liq}(\omega) = C_2 \left( F^{-1} - 1 - i\frac{\omega}{\omega_0}\frac{1}{Q} + \frac{\omega^2}{\omega_0^2} \right)^{-1} - \frac{1}{AG} \,. \tag{S5}$$

The bulk modulus (with the "subtracted" hydrodynamic flow in the filling pipe) is obtained as follows

$$K_S(\omega) = \frac{V}{C_{\rm liq}(\omega)} \,, \tag{S6}$$

where $C_{\rm liq}$ is given by Eq. (S5).

The procedure is illustrated in Fig. S3, where both the pure viscous correction and the correction including the frequency-dependence of the viscosity is shown for 2E1H. For comparison, we show how the pure viscous correction works for a non-associated molecular liquid, the commercial silicone oil DC704 [S5].

## IV. COMMENTS ON THE POISEUILLE FLOW ASSUMPTION

In fluid dynamics, the Poiseuille law relates the flowrate, $\dot{V}$ to the pressure drop $\delta P$ over the pipe

$$\dot{V} = R_{\rm hyd} \delta P \,, \tag{S7}$$

where the hydrodynamic resistance $R_{\rm hyd}$ inversely proportional to the fluid's viscosity, $\eta$. The constant of proportionality is the geometrical constant given by Eq. (S3).

The assumptions of Eq. (S7) are that 1) the liquid is incompressible and Newtonian, 2) the flow is laminar, 3) there is no acceleration of fluid in the pipe and 4) the pipe has constant circular cross-section and the length of the pipe is substantially longer than its radius.

In our case we do not have a constant flow, but a pulsating flow where the frequency of the pulsations varies from 1 mHz to 10 kHz. Of course assumption of zero acceleration no longer holds, but the requirement of a laminar flow translates into the frequency of pulsations being sufficiently low so that a parabolic velocity profile has time to develop during each cycle. In that case the Poiseuille equation hold to a good approximation. This is fulfilled when Womersley number, $\alpha$, is small. Wormersley number is given by

$$\alpha = a\sqrt{\frac{\omega\rho}{\eta(\omega)}} \,. \tag{S8}$$

where $\omega$ is the angular frequency, $\rho$ is the density, $\eta$ is the frequency-dependent viscosity and $a$ is the radius of the pipe.

In Fig. S4 the Womersley number is shown as a function of frequency and temperature in the case of 2E1H and clearly shows that $|\alpha| < 1$ at all temperature in the relevant frequency range, and thus assumptions two and three are met.

The filling pipe is cylindrical, the radius is approximately $a \approx 1.5$ mm, while the length is approximately $L \approx 4$ mm. The requirement that $a/L \ll 1$ is maybe not completely met. However, when in a pulsating flow the problem is smaller at high frequencies. In agreement with this, we observe that the correction building on the Poiseuille flow assumption gradualy breaks down for low frequencies (i.e., for frequencies lower than the peak frequency of the Helmholtz mode, see Fig. S3).

The Poiseuille equation has been shown to work (surprisingly) well for supercooled molecular liquids at the frequency ranges and pipe dimensions explored here [S5].

## V. DETERMINING THE GEOMETRIC FACTOR

The geometric factor in Eq. (S3) that enters the calculation of the Poiseuille flow correction consist of the length, $L$, and diameter, $a$, of the filling tube. In principle, these quantities can be determined by measuring directly the dimension of the tube. In practice, this is not so easy since the filling tube is hidden at the bottom of a larger liquid reservoir, and so it is difficult measure the tiny dimensions accurately inside measuring cell.

Instead we 'calibrate' the geometrical constant with another set of shear and bulk modulus data measured in the same experimental set up, and – in the case of the bulk modulus – in the same measuring cell. The data are

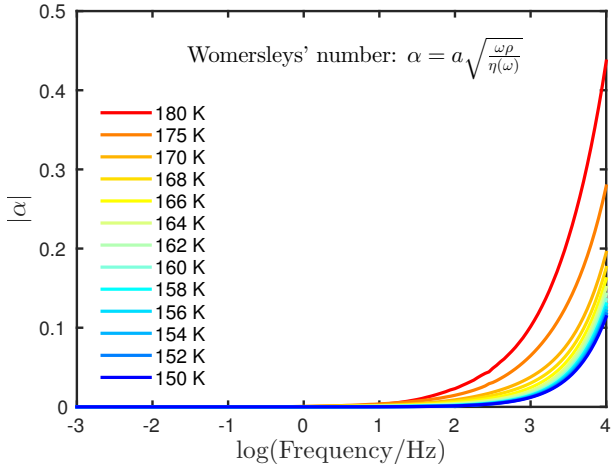


FIG. S4: Womersley number calculated as a function of frequency for 2E1H at several temperatures. When $\alpha$ is small ($< 1$), it means the frequency of pulsations is sufficiently low that a parabolic velocity profile has time to develop during each cycle, and the flow will be very nearly in phase with the pressure gradient. The flow will then be given by Poiseuille's law to a good approximation, using the instantaneous pressure gradient.

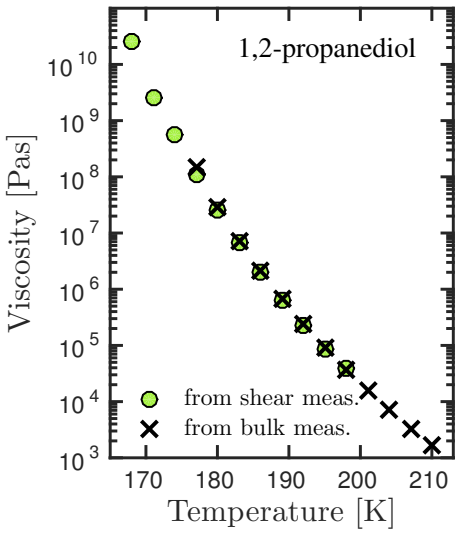


FIG. S5: Shearviscosity of 1,2-propanediol measured directly as the low-frequency plateau of the real part of the complex shearviscoity, $\eta = G/i\omega$, and as inferred from the Poiseuille flow in the bulk transducer described in the text (for more details, see Ref. [S5]). Data are from Ref. [S8]. This determines the geometric factor of the translation between hydraulic resistance and shear viscosity for that particular transducer (named q10 for internal reference) to $A = 3.6 \times 10^9$ m$^{-3}$.

1,2-propandiol data published in Ref. [S8]. In Fig. S5 we show the static shear viscosity as determined from the low-frequency plateau value of the frequency-dependent viscosity measured in the PSG (green circles) as well as the static shear viscosity determined by the Helmholtz mode [S5] with a geometric factor adjusted, so the two curves coincide. The geometric factor used for correcting the low-frequency side of the bulk modulus spectra was $A = 3.6 \times 10^9$ m$^{-3}$. This values agrees qualitatively with the number found when inserting the values for radius and length stated in Sec. IV above in Eq. (S3).

[S1] B. Igarashi, T. Christensen, E. H. Larsen, N. B. Olsen, I. H. Pedersen, T. Rasmussen, and J. C. Dyre, Rev. Sci. Instrum. **79**, 045105 (2008).

[S2] B. Igarashi, T. Christensen, E. H. Larsen, N. B. Olsen, I. H. Pedersen, T. Rasmussen, and J. C. Dyre, Rev. Sci. Instrum. **79**, 045106 (2008).
[S3] T. Christensen and N. B. Olsen, Rev. Sci. Instrum. **66**, 5019 (1995).
[S4] T. Christensen and N. B. Olsen, Phys. Rev. B **49**, 15396 (1994).
[S5] T. Hecksher, N. B. Olsen, K. A. Nelson, J. C. Dyre, and T. Christensen, J. Chem. Phys. **138**, 12A543 (2013).
[S6] B. Jakobsen, C. Maggi, T. Christensen, and J. C. Dyre, J. Chem. Phys. **129**, 184502 (2008).
[S7] C. Gainaru, R. Figuli, T. Hecksher, B. Jakobsen, J. C. Dyre, and M. A. B. Wilhelm, Phys. Rev. Lett. **112**, 098301 (2014).
[S8] D. Gundermann, K. Niss, T. Christensen, J. C. Dyre, and T. Hecksher, J. Chem. Phys. **140**, 244508 (2014).